Three-Dimensional Structure of the Surface Layer Protein of *Aquaspirillum serpens* VHA Determined by Electron Crystallography

M. R. DICKSON,[1] K. H. DOWNING,[2]* W. H. WU,[3] AND R. M. GLAESER[2]

Biomedical Electron Microscope Unit, University of New South Wales, Sydney, Australia[1]; and Donner Laboratory, Lawrence Berkeley Laboratory,[2] and Department of Biophysics and Medical Physics, University of California,[3] Berkeley, California 94720

The three-dimensional structure of the protein which forms the S layer of *Aquaspirillum serpens* strain VHA has been determined by electron microscopy. Structures have been reconstructed to a resolution of about 1.6 nm for single-layered specimens and about 4 nm for two-layered specimens. The structure, which has hexagonal symmetry, consists of a core in the shape of a cup, with six projections arising from the rim of the cup to join adjacent subunits at the threefold symmetry axes. The model is consistent with edge views of the S layer which have been obtained in this and other work. It is now clear from this work and from three-dimensional reconstructions of other bacterial S layers that a wide diversity exists in the morphology of surface layers.

Many species of bacteria have a surface (S) layer of macromolecules which encloses the rest of the cell wall; Sleytr and Messner (15), for example, list in their review 66 gram-negative eubacteria, 44 gram-positive eubacteria, 27 archebacteria, and 5 cyanobacteria in which surface layers have been found. S layers are generally thought to be involved both with retention of the shape of the bacterium and restriction of access of certain solute species to the cell (2, 15).

The surface layer in *Aquaspirillum serpens* VHA was initially identified by Murray (12), who observed an array of "roughly hexagonal rings" each having a central "hole" and "up to six radial projections" which formed triads in the form of a "Y." Buckmire and Murray (4) proposed a morphological model in which monomers of molecular weight 48,000 were associated as trimers having a threefold, spokelike structure. Trimers were in turn paired as hexamers to produce a morphological unit consisting of a large globular structure with a central hole and six Y linkers. Three of the Y linkers were located at one level in the structure, and three were located at a second level. Glaeser et al. (7) proposed a different model based on electron microscopy in which the morphological unit was a hollow cylinder flared out at one end to form six spokes. The center-to-center distance between units in the array was given as 14.5 nm, the height of each unit was 15.5 nm, the width of the cylinder below the flare was 8.5 nm, and the diameter of the hole was 2.5 nm. Both of these models are based on face and side views of negatively stained material. Although informative, models based on only two views are not as satisfactory as proper three-dimensional reconstructions.

The recent availability of single-layered arrays of the surface layer protein from *A. serpens* VHA (W. H. Wu, Ph.D. thesis, University of California, Berkeley, 1983) has enabled us to obtain a high-quality, three-dimensional reconstruction of negatively stained specimens. Single layers proved far more suitable for reconstruction than the col-

lapsed vesicles on which previous observations were made. The results confirm, with additional detail, the model proposed by Glaeser et al. (7). Although considerable flattening of the structures is observed along the vertical axis, the basic topology seen in the three-dimensional reconstruction is still consistent with projections observed in face and side views of frozen hydrated specimens.

MATERIALS AND METHODS

A. serpens VHA was supplied by R. G. E. Murray (Department of Bacteriology and Immunology, University of Western Ontario, London, Ontario Canada). Cells were grown by the procedure of Buckmire and Murray (3) in medium containing 0.1% yeast extract (Difco Laboratories), 0.1% peptone (Difco), 0.05% anhydrous sodium acetate (Mallinckrodt, Inc.), 0.025% anhydrous calcium chloride (Baker and Adamson), 0.025% $MgSO_4 \cdot 7H_2O$ (Mallinckrodt, Inc.), and 0.005% L-cystine (pH 7.6). Harvesting and isolation of cell wall fragments were performed as described by Buckmire and Murray (3). Formation of large, coherent crystalline patches of the protein was induced by several cycles of heating (60°C, 4 to 6 h) in 0.5 mM Tris (pH 7.4 measured at 20°C) containing 5 mM calcium chloride.

Negatively stained specimens were prepared immediately before microscopy by placing a drop of suspension on a carbon-Formvar film on a grid, mixing well with a drop of phosphotungstic acid, blotting, and allowing to dry for 10 min. Electron micrographs were recorded with an underfocus value of no more than 600 nm, such that the first zero in the contrast transfer function always occurred outside a radius corresponding to 0.7/nm.

Single-layer arrays could readily be distinguished by the amount of staining and were recognizably different from membrane patches and double-layered arrays which were found in the same preparations. A number of series of micrographs, all at a magnification of ×50,000, were recorded of suitable patches tilted up to 63°. The increment in tilt angle was either 5 or 10° within each tilt series. Excessive

* Corresponding author.

illumination of the specimen was avoided, but low-dose imaging was not attempted.

Frozen-hydrated specimens were prepared using the double carbon film method of Jaffe and Glaeser (9) and were viewed in a JEOL 100B microscope at a temperature of −125°C.

Optical diffractometry was used to select the micrographs showing the highest resolution and to identify areas showing the best order in the crystal lattice. Seven tilt series were judged good enough for use in producing the final model. Data from micrographs of 10 untilted specimens were merged to produce an ideal set of zero-tilt data. A total of 45 micrographs of tilted specimens contributed data to the final model.

Images were digitized with a Perkin-Elmer PDS 1010M flat-bed microdensitometer with a square 25-μm aperture (0.5 nm on the specimen at ×50,000 magnification). Arrays of 512 by 512 pixels were scanned at intervals of 25 μm. Such an array corresponded to at least 120 unit cells. All films were scanned in the same orientation, emulsion side up, with the nominal tilt axis parallel to the X axis of the scanning raster.

Image processing was carried out on a VAX 11-780 computer with software partly derived from the MRC system (1) and partly written by D. A. Grano at Berkeley. Fourier transforms were calculated and displayed for indexing and initial determination of the coordinates of the reciprocal lattice. Areas of the transforms (amplitudes and phases) around each of the predicted reciprocal lattice points were displayed so that the peak positions could be accurately determined. Although many of the spots fell on a single point of the calculated transform, spots were often found to be split between two or more of the transform points, such as when the reciprocal lattice point fell between points of the transform. Refinement of the reciprocal lattice coordinates was carried out until the splitting of the amplitudes from most of the fairly strong spots followed the distribution as predicted from the position of the reciprocal lattice point with respect to the transform points.

To handle the large amount of data contained in the many transforms, peak amplitudes and phases were automatically extracted from the transforms by a program which was written to mimic the sequence of judgments applied when the data are extracted manually. The sequence was as follows. Points of the transform within a radius of 1.4 pixels of the calculated reciprocal lattice point were examined, and the two highest amplitudes were noted. The average amplitude in a 9- by 9-pixel region surrounding the reciprocal lattice point was also calculated. The amplitude and phase of the structure factor were then determined using the first of the following criteria which could be met.

(i) If the ratio of the two highest values was greater than 1.5, and the highest amplitude was greater than 2.5 times the local background, the amplitude and phase of the highest point were selected.

(ii) If both the highest values were greater than 1.6 times the local background, these two values were used by taking the vector sum.

(iii) If the highest amplitude was at the point closest to the calculated reciprocal lattice point and was at least 1.5 times the background, the point was selected.

(iv) If none of the above criteria could be met, all points within 1.4 pixels of the calculated reciprocal lattice point were used by calculating the vector sum of the individual points, with weighting for the distance from the calculated lattice point.

The first three of these criteria follow the judgments that are generally made in selecting valid diffraction spots. The values used in selecting among the various criteria were based on properties of the noise distribution in the transform (8) and were adjusted to produce results most similar to those obtained with the manual procedure. The automated procedure was carefully monitored, and in fact in almost every case the same values for the structure factor were selected as would have been used in a manual treatment. Even when no diffraction spots are detectable, it is still possible that a spot may be spread among several transform points. In this case, the phases at these points will be correlated. A vector sum over the points will tend to point in the direction of the true phase, although the angle will be influenced both by the adjoining points which do not contribute to the diffraction spot and by the noise in the real spot.

For each case a figure of merit was calculated from the peak height and the known characteristics of the noise distribution in the background around the lattice point (8; K. H. Downing, D. A. Brillinger, and R. M. Glaeser, manuscript in preparation). The figure of merit represents a systematic measure of the reliability of the experimental data. A figure of merit of 1.0 would imply the absence of any possible error in the phase. Measurements with a figure of merit of 0.7 could be expected to contribute as much to the error in the final structure as to the true structure. For each reciprocal lattice point considered, the program produced a list containing amplitude, phase, and figure of merit.

Warping or bending of the support film is found to introduce specimen tilts that are often 5° or more, so the stage goniometer setting and tilt axis cannot give reliable values for the actual tilt angle and axis. Tilt angles and axes were determined using the ratio of a* and b* vector lengths and the included angle, by the procedure of Shaw and Hills (13). This procedure is quite accurate for tilts greater than about 20°. Plots on polar graph paper of tilt angle and axis for the high-tilt images within a given tilt series fell quite accurately on a straight line, which could be extrapolated to give reliable estimates for the tilt angles and axes in the range of 5 to 20°.

RESULTS

Molecule in projection. The single-layer patches were quite highly ordered, as opposed to the collapsed vesicles which had been used in previous work. Figure 1a shows a section of a micrograph of one of the arrays, nominally untilted. The computer-generated Fourier transform is shown in Fig. 1b. The strongly chiral appearance of the transforms of the single-layer arrays differs from the mirror symmetry of transforms of the collapsed vesicles. All of the highly ordered arrays used in this work displayed the same handedness of the transform, indicating that all had adhered to the grid in the same orientation.

The resolution of images in this projection often extended to around 1.3 nm. With careful use of minimum exposure techniques, diffraction spots were occasionally found at resolutions out to around 0.6 nm in images of specimens prepared and examined at low temperature (Wu, Ph.D. thesis).

Figure 1c is a filtered image of Fig. 1a, obtained by masking out 5- by 5-pixel boxes around each diffraction spot in the Fourier transform and then performing an inverse transform. Several features of this image are different from filtered images obtained from the vesicles (7), but the inter-
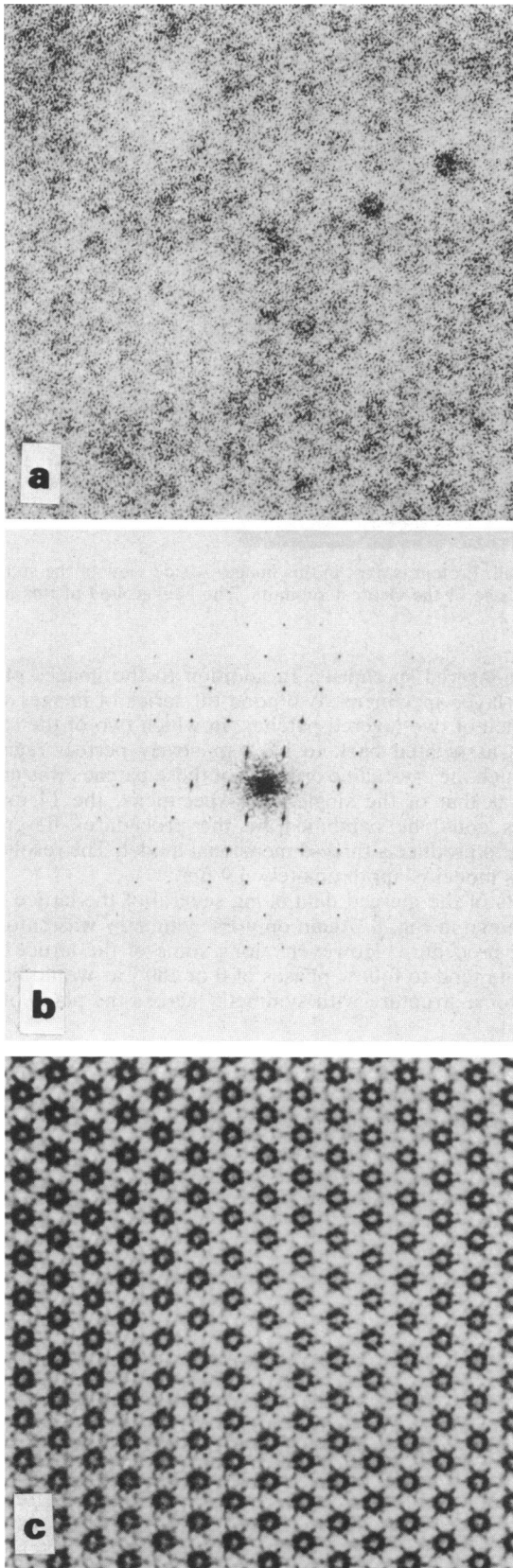
FIG. 1. (a) Representative example of an untilted, negatively stained specimen of *A. serpens*. (b) Fourier transform of the micrograph, showing a strongly chiral, sixfold symmetry pattern

pretation of densities seen in this projection requires knowledge of the three-dimensional structure.

Side views of the molecule. In previous work (7) it had been possible to obtain side views of the molecule at the edges of membrane vesicles, both in negatively stained specimens and in frozen hydrated specimens. In fact, the structure of the model was based largely on the interpretation of such views. Similar views were also obtained in this work. One such view, obtained from a frozen hydrated preparation, is shown in Fig. 2. This image is quite consistent with those presented earlier, giving the impression that the molecule is shaped something like a mushroom with a hole passing through the stalk.

Data merging for tilted specimens. Images of the tilted specimens were brought to a common phase origin with the untilted image by minimizing the differences in phases derived from an image being aligned and phases previously determined along the lattice rods, within a distance along the rods corresponding to the reciprocal of the specimen thickness. When P6 symmetry was enforced during the merging, the average of the root mean square phase errors for adding each image to the established data set was 13°. In this procedure data could be selected on the basis of the figure of merit of the individual measurements, so that any data point with too small a figure of merit would not enter into the phase origin determination. The minimum figure of merit was generally set to 0.7 to 0.8, although it was noted that even data points with a figure of merit of 0.5 were frequently consistent with the other data.

Along each reciprocal lattice line, smooth curves were then fit to describe the variation in phase and amplitude with z^*. The results of merging the tilt series data and defining the amplitude and phase along representative lattice rods are illustrated in Fig. 3. For the strong diffraction spots, the self-consistency of the data is extremely good. As is normal, the reliability of the data becomes worse at higher resolution. The reliability of the fit of the smooth curves to the data along the lattice rods can again be expressed in terms of a figure of merit. Such figures of merit were estimated by considering the scatter of the data within sections of the lattice rods corresponding to the reciprocal of the specimen thickness. The figures of merit were well above 0.9 on most lattice rods to a resolution of at least 3 nm. On most of the lattice rods we were able to use data with a high degree of confidence (figure of merit of >0.7) to a resolution of around 1.6 nm. Figure 4 shows the limiting resolution on each of the lattice rods.

The real space structure was then calculated on parallel sections of the unit cell by inverse transformation of the three-dimensional Fourier transform. Contour plots of the density on several of the sections are shown in Fig. 5 and 6. Figure 5 shows sections parallel to the plane of the array (Fig. 5c) near the middle of the body of the structure, showing the connection of six dense regions into an annular structure at this level; (Fig. 5b) just above the top of the body, where the six dense regions are separated from each other and six other dense segments arise to form the Y linkers; and (Fig. 5a) near the level of the greatest contact of the Y linkers.

Some aspects of the structure are more easily seen in Fig.

characteristic of the single-layered arrays. (c) Filtered image of the micrograph, obtained by masking regions in the vicinity of the diffraction spots of the transform and performing an inverse transform.
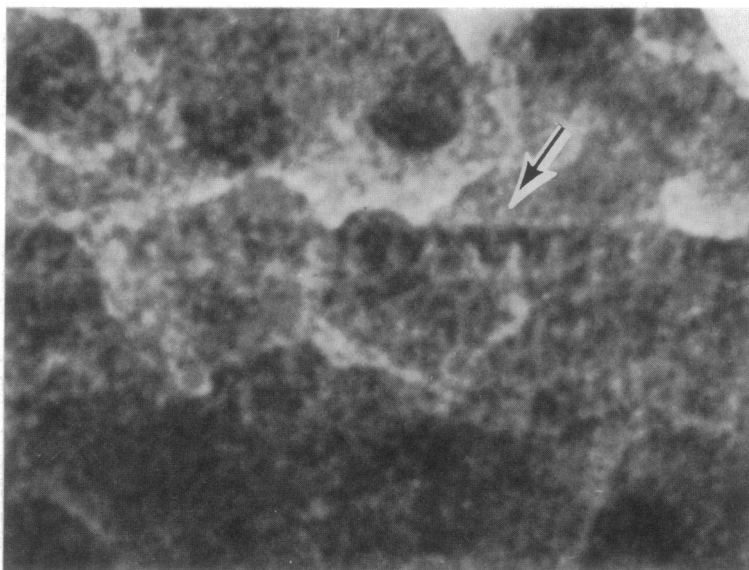
FIG. 2. Electron micrograph of a frozen hydrated preparation of the cell wall. Protein is dark in this image. A side view of the subunits of the S layer is obtained where the wall is folded over. The arrow indicates one of the clearest subunits. The background of this image contains islands of condensed ice.

6, a section perpendicular to the plane of the array. This section spans one unit cell in an orientation chosen to pass near the highest density of the Y linkers. The approximate area of this section included within the boundary chosen for the three-dimensional model is indicated by the shaded region. It can already be seen that there is no continuous pore passing through the center of the structure.

Three-dimensional model derived from the merged data. Three-dimensional surface representations were generated by using an implementation of the MOVIE.BYU graphics system developed in the Department of Civil Engineering at Brigham Young University. The surface of the molecule was selected in this procedure to show the connectivity of the molecule, at a level corresponding to 20% of the maximum calculated density.

Several views of the three-dimensional reconstruction are shown in Fig. 7. Figure 7a and b show the central part of the structure. These views extend out into the Y linkers to the position of the unit cell edge, as in Fig. 5. These figures were calculated by computationally "smoothing" the surface. Representations of such models are more commonly generated with sections of balsa wood or other solid material. Figures 7c is such a computer-generated, "balsa wood" model. To show both the connections between Y linkers and a view of the inside of the model, this view was calculated including 1.5 unit cells in each direction.

The three-dimensional model is a squat cylinder 6.0 nm high and 8.0 nm in outer diameter. The center of the cylinder is hollowed into a cup 3.5 nm deep and 3.0 nm in diameter. The wall of the cylinder includes six denser rods that follow rather steep right-hand spiral paths. In the vicinity of each spiral density, 2.0 nm above the base, slender projections radiate outward, terminating in dense regions were Y linkers from neighboring units make contact. The Y linkers border depressions about 1.5 nm in diameter centered on the threefold axis where they meet.

Four separate reconstructions have been calculated: two using (separately) the best two tilt series, one combining these best two series, and one using all seven tilt series. All models were remarkably similar in all details.

Two-layered specimens. In addition to the images of the single-layer specimens, two good tilt series of images were obtained of two-layered patches, in which two of the single layers associated back to back in nearly perfect register. Although the crystalline ordering of these patches was not as good as that of the single-layer specimens, the 14 micrographs could be combined by the procedures described above to produce a three-dimensional model. The resolution of this model is approximately 4.0 nm.

Plots of the merged data along several of the lattice rods are shown in Fig. 8. Again only P6 symmetry was enforced in the procedure. However, along some of the lattice rods the data tend to follow phases of 0 or 180°, as would be the case for a structure with symmetry across the plane of the crystal.

A cross section of the two-layered model is shown in Fig. 9, and two views of the three-dimensional structure are shown in Fig. 10.

In the absence of specimen distortions such as those due to flattening and drying artifacts, one would expect the top and bottom halves of the model to appear the same, even though no symmetry across the midsection was imposed during the reconstruction. The influence of flattening is especially prominent on the bottom. Otherwise the features of this model are remarkably similar to those of the single layer.

DISCUSSION

The data used in synthesizing the final model are heavily overdetermined. Virtually identical models were obtained with data subsets containing about one-sixth of the full data. Low values of the residual phase errors of around 10 to 15° were found on merging data from the different tilt series into the full set. The low phase residuals attest to the constancy of the specimen structure throughout the experiment and give confidence in the final model as an accurate representation of the negatively stained structure. We should, however, point out several sources of structural artifacts which are present to some degree in all such work.

(H,K) = (1,2)

(H,K) = (2,2)
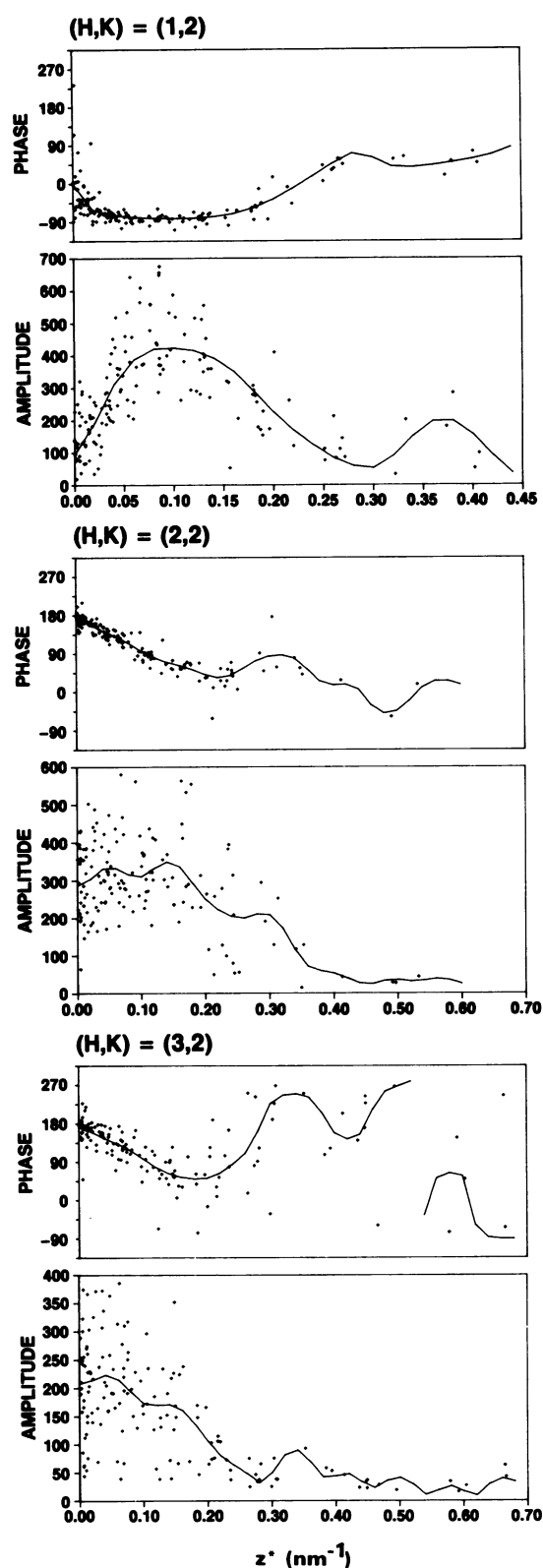
(H,K) = (3,2)

z* (nm⁻¹)

FIG. 3. Representative examples of the three-dimensional structure factors obtained from the single-layer specimens of the S-layer protein. The variation of the amplitude of the Fourier transform and its phase along reciprocal lattice rods is plotted for three representative rods. The smooth curves are generated as a fit to the observed data points with the constraint that the curves cannot change more
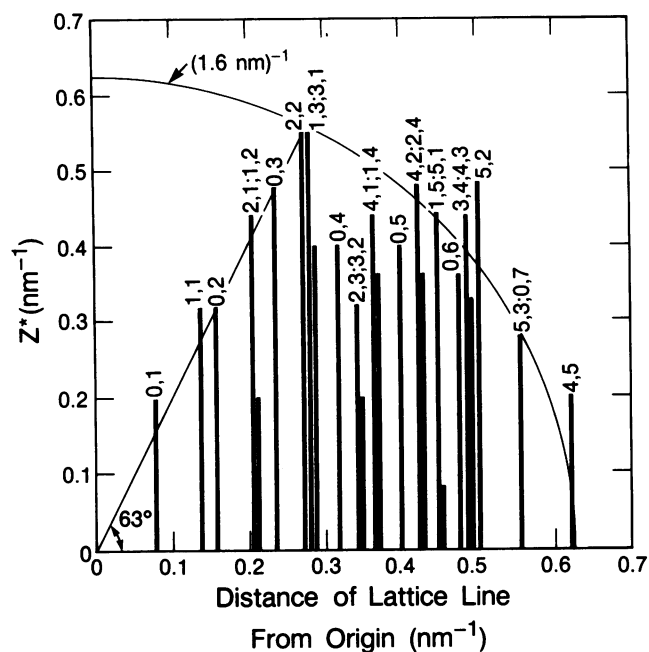

Distance of Lattice Line

From Origin (nm⁻¹)

FIG. 4. The full area of reciprocal space for which data were used in computing the three-dimensional density map for the single-layer specimens. Solid lines are plotted over the range of z* for which amplitudes and phases of the structure factor were obtained for each reciprocal lattice rod. The Miller indices of each rod are shown above the corresponding solid lines, with the convention that rods with index h,k and index k,h are shown slightly displaced from one another, even though they really should be placed at exactly the same distance from the origin. The k,h rod is always shown to the right of the h,k rod.

According to the description of Glaeser et al. (7), each unit in the array is 15.5 nm high with a 2.5-nm hole. Our current model agrees quite well with the previous one in general appearance. The closure of the hole at the bottom is perhaps the most significant new feature of the model that had not been anticipated on the basis of side views of the specimens.

Our three-dimensional reconstruction is, however, noticeably shorter than the values quoted in previous measurements, 11.0 versus 15.5 nm. Some compression is not unexpected in view of the specimen flattening that is generally observed in negatively stained specimens (11). In fact it appears that the lower part of the molecule may bulge out as a result of the flattening. If this lateral (i.e., "radial") expansion is significant at the level of the Y linkers as well, it could result in tilting of the Y linkers up from a more horizontal position, thus accounting in part for the unexpected, vertically oriented prolate ellipsoids of density near the threefold axis. Such a distortion of the base could also tend to produce a closure of a pore passing through the base of the native molecule.

The surface defining the model shown in Fig. 7 encloses 600 nm³. Assuming a protein density of 1.3 g/cm³, this volume corresponds to 60% of the mass expected in a hexamer of 140,000-dalton subunits. The absence of the remaining mass is at least in part attributable to disorder in the specimen, which in turn may result from both radiation damage and the effects of flattening during negative staining.

rapidly than would be consistent with the specified thickness of the specimen.
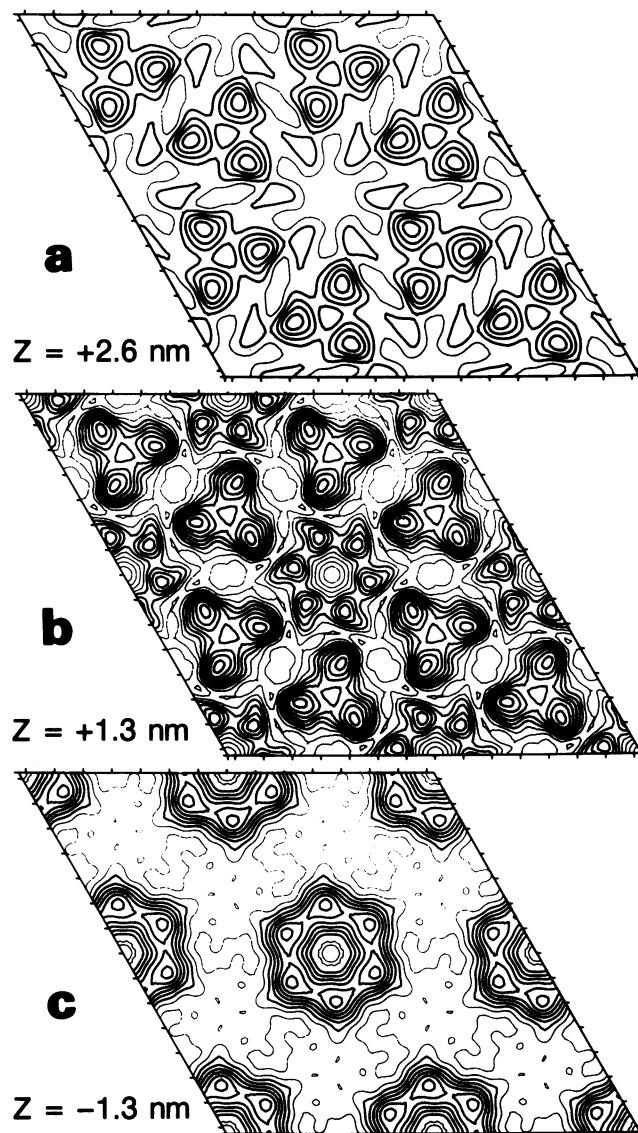
FIG. 5. Contour plots of three sections of three-dimensional reconstruction, along planes that are parallel to the S-layer plane: (a) a section at a level near the greatest contact of the Y linkers; (b) a section just above the top of the body of the molecule, showing the six Y linkers and the six other bodies of mass that project from the top; (c) a section near the middle of the body of the molecule. The center-to-center distance between hexagonal subunits is 14.5 nm.
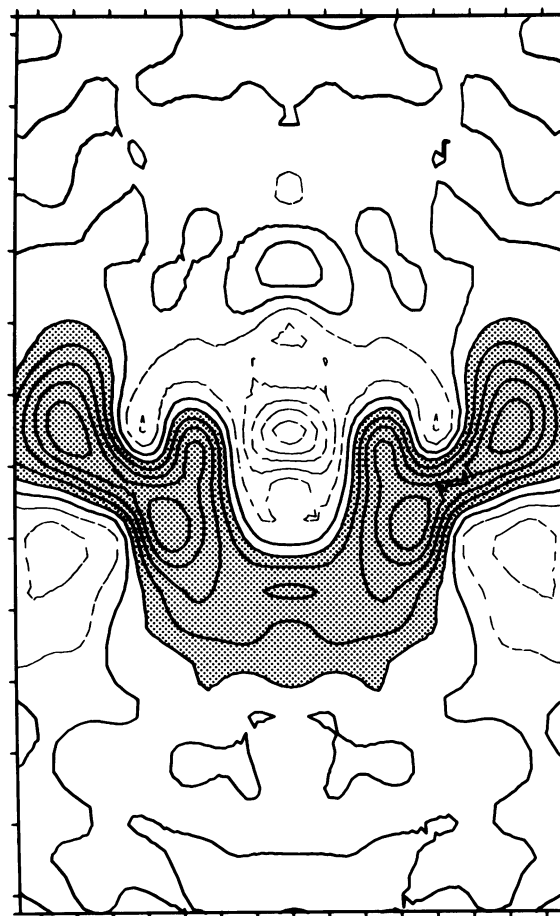

FIG. 6. Contour plot of a vertical section through the Y linkers. The plot includes an area of 25 by 8.7 nm. The shaded area corresponds approximately to that enclosed by the surface representations of the three-dimensional model of Fig. 7.

The apparent size and enclosed volume of models of this type depend on the choice of the density level which is used to represent the surface. The choice of a lower density for the surface would increase the volume and the height, but would also include areas of the reconstruction which are rather poorly defined. For example, the Y linkers would extend farther up into a region where the density varies in a rather noisy and erratic fashion (Fig. 6).

A small dense plug "floats" over the mouth of the central cavity (Fig. 6). Baumeister et al. (1a) have found that such plugs can arise as artifacts due to the incomplete character of data for specimens tilted within a range of ±60°. We have therefore not included this feature in the three-dimensional displays. Baumeister et al. (1a) also point out that the closure at the bottom of the cup can, under some conditions, arise as

an artifact in the reconstruction. In the present instance, however, the closure of the structure at the bottom of the cup in both the single-layered and the double-layered specimens indicates that this feature is most likely a real characteristic of the structure.

The degree of similarity between the basic features of the single-layered model and the top half of the two-layered model was unanticipated, given the lower resolution of the latter model. To some extent this similarity is due to the relatively low amplitude of most of the data beyond about 3-nm resolution. The edge definition is nevertheless much clearer in the single-layered model, e.g., comparing Fig. 6 and 9, although the overall distribution of density is very similar in the two models. The greatest differences are seen in the Y linkers. Even in these regions, though, the difference in appearance of the surface would have been reduced by the choice of a higher-density cutoff in the upper half of the two-layered model and a lower-density cutoff in the lower half.

Comparison of bacterial surface layer models. Apart from the reconstruction described here, several other three-dimensional reconstructions of bacterial surface layers have been published in some detail. Of these, the S layer of *Methanospirillum hungatei* on the tubular cell sheath (14) is unusual in that it consists of roughly spherical subunits arranged in an orthorhombic array. All others consist of
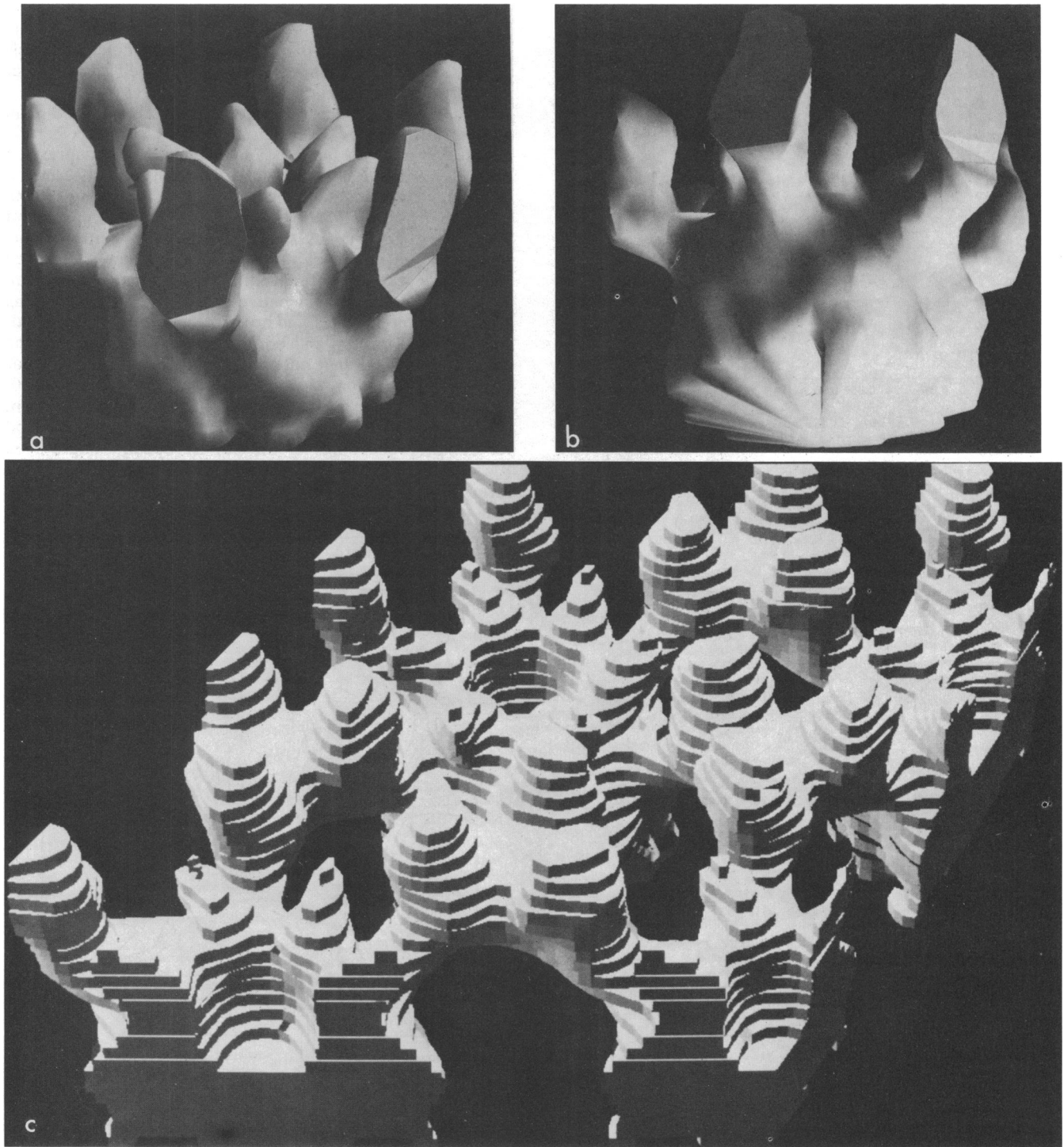
FIG. 7. Computer-generated views of the three-dimensional model. (a) "Smoothed" model of the body of the molecule, showing two sets of six projections which emanate from near the top of a hollow cup; (b) the same as a, but viewed from bottom; (c) a computer-generated simulation of a balsa wood model, including 1.5 unit cells in each direction, showing the connectivity between molecules.

morphological units that are packed with P6 symmetry and which possess a cavity centered on the sixfold axis of symmetry.

The reconstruction of the S layer of *Deinococcus radiodurans* (Baumeister et al., in press) has a central, globular body with a deep depression opening toward the

cell membrane. Linkers along twofold symmetry axes join the units in a hexagonal array with cell dimensions of about 18 nm. The linkers are nearly parallel to the membrane, roughly in the center of the model.

The structure of the S layer of *Sulfolobus acidocaldarius* (6, 16) is a very open one. The unit cell dimension is 22 nm.

(H,K) = (1,1)

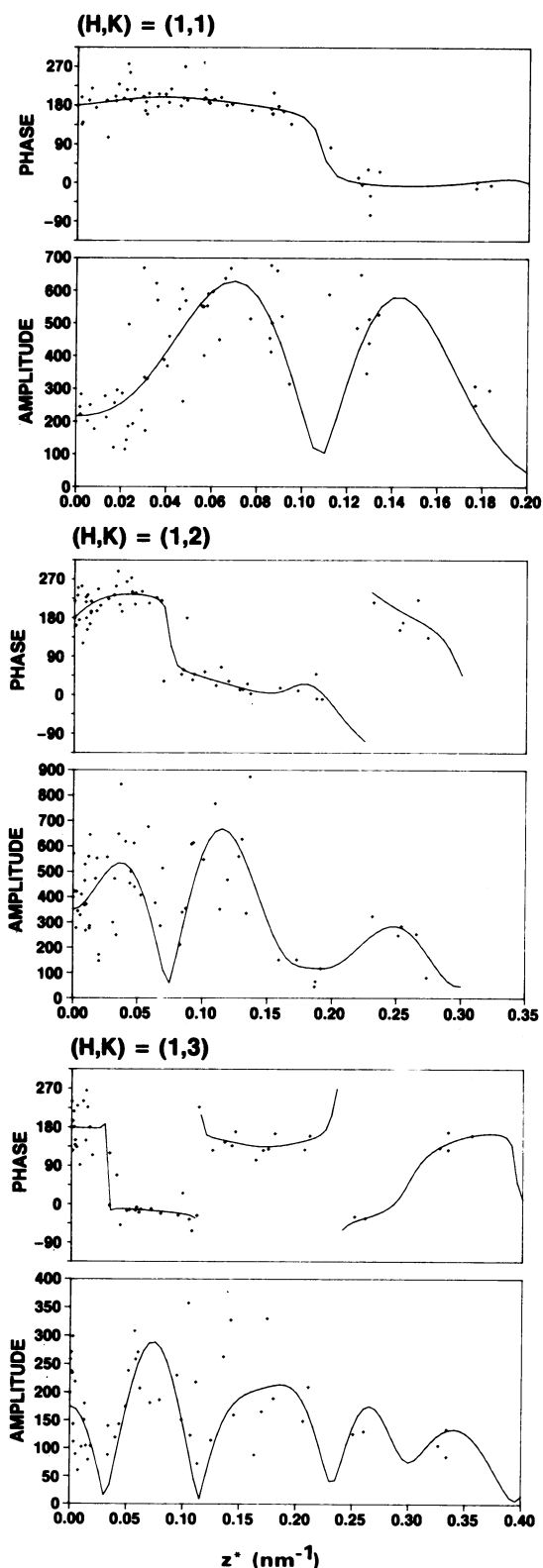**(H,K) = (1,2)**

(H,K) = (1,3)

z* (nm⁻¹)

FIG. 8. Representative examples of the three-dimensional structure factors obtained from the two-layered specimens. The amplitude and phase are plotted for three reciprocal lattice rods. Note that the computer program which fits curves to the data points tends to force the amplitude toward zero at points where the phase changes rapidly.

The protein molecular weight in this case is 140,000 to 170,000. A large floorless chamber 18.5 nm wide and 8 nm deep opens extracellularly through a 5-nm hole. Channels 2.5 nm in diameter communicate between the large chamber and 4.5-nm holes on the threefold axes.

Chlamydia trachomatis (5) has an S layer composed of an annular structure of six subunit domains around a central depression 10 nm in diameter and 8 nm deep. The depression opens towards the cell membrane. The unit cell is 17.5 nm on edge, and the molecular weight of the protein is only 39,500.

The S layer of *Synechocystis* sp. (10) is composed of regular hexagonal arrays, the dimension of the unit cell being 15.2 nm. The monomer proteins form hexamers arranged around a central hollow space that is 2.5 nm in diameter and 10 nm deep. The linkers between the hexamers are along twofold symmetry axes and are located approximately midway between the top and bottom of the protein layer. The central hollow is open only extracellularly. The molecular weight of the monomeric protein was estimated as 100,000.

The *Bacteroides* sp. organism (S. Hovmöller, A. Sjögren, G. Farrants, M. Haapasalo, H. Ranta, K. Lounatmaa, and K. Tanta, Proceedings of the 8th European Congress on Electron Microscopy, Budapest, p. 1513, 1984) has an S layer 15 nm thick, displaying P6 symmetry with lattice dimensions of 19.5 nm. A 5-nm-diameter pore is centered on the sixfold axis, and smaller pores 5 by 2.5 nm are located
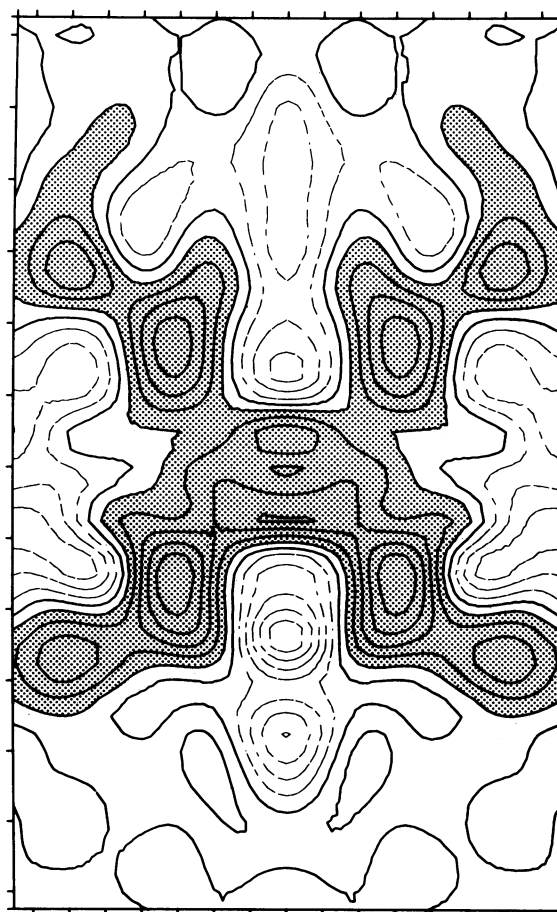

FIG. 9. Contour plot of a vertical section through the density map of the two-layered specimen. The Y linkers on the top section are rotated ~15° from those on the bottom. This section is in a plane which passes through parts of both Y linkers.
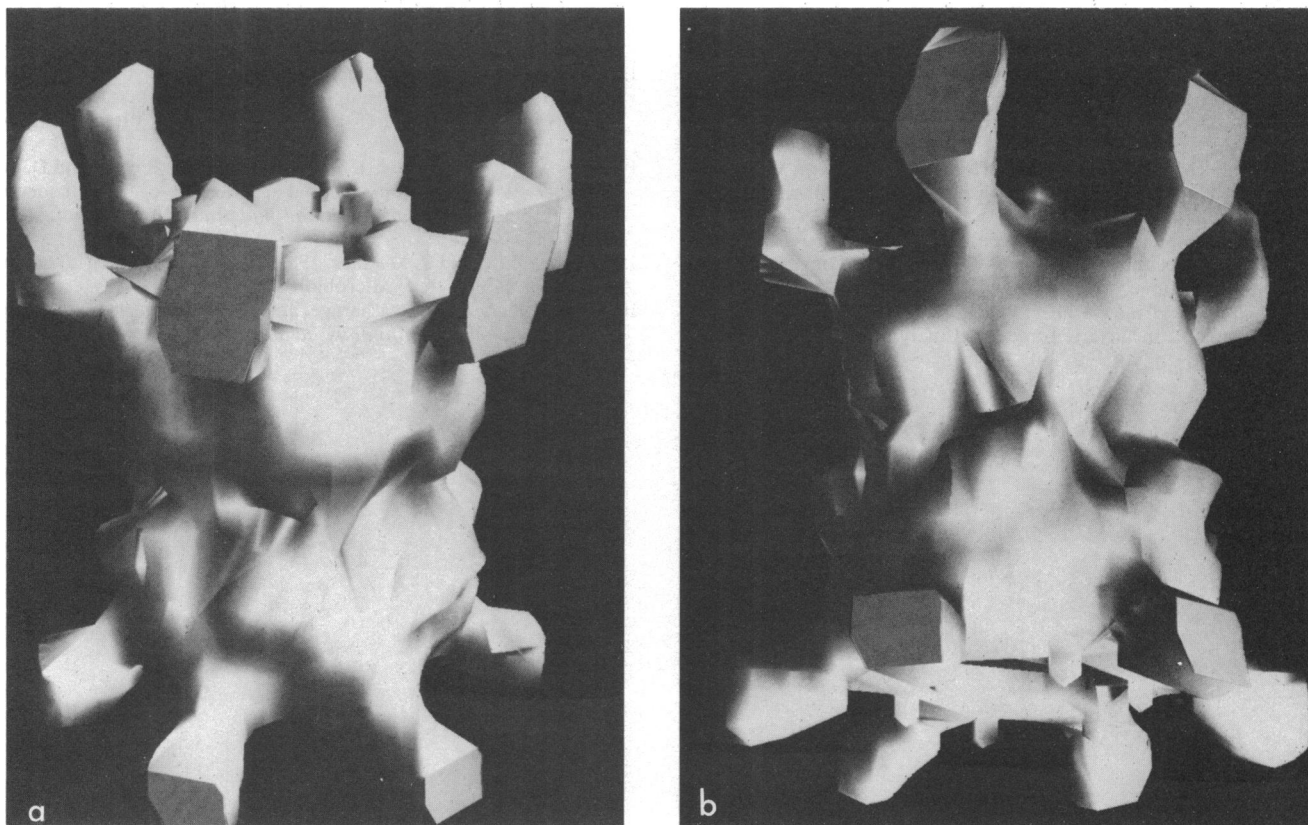
FIG. 10. Computer-generated views of the three-dimensional reconstruction of a two-layered specimen viewed (a) from above and (b) from below.

between the threefold and sixfold axes. No estimate of the monomeric molecular weight is available.

In addition to these studies of three-dimensional structure, quite a few bacterial S layers have been studied in projection. Many differences have been observed among these. The subunits are usually, but not always, packed on a hexagonal or tetragonal lattice. Lattice spacings vary between 5 and 25 nm, and molecular weights of the monomers comprising the lattice vary from 12,000 to 200,000 (15). Adjacent subunits are connected by linkers which are sometimes observed to lie near twofold axes (delta linkers) and sometimes near threefold axes (Y linkers).

It had at one time been reasonable to suppose that bacterial surface layer proteins would tend to have quite similar structures, since they might reasonably derive from a common precursor gene. The idea that the structures might be homologous to a large degree has been easy to rationalize, or to be made consistent, with images that correspond only to two-dimensional projections in the direction perpendicular to the plane of the S layer. For example, of the S layers with hexagonal symmetry, most can be interpreted as being a roughly globular or cylindrical body, sitting on a sixfold symmetry axis of the array with a hole passing through the center. The information now available from three-dimensional reconstructions shows, on the other hand, that the molecular morphologies of the proteins that make up the S layers are not, after all, similar. The cavity at the sixfold axis may be a closed cup, an inverted cup, a pipe with top and bottom openings of different diameters, or a chamber with perforated walls. The linkers which join adjacent units show similar diversity. The available work on three-dimensional

reconstruction of the molecular morphology of these layers therefore serves to deepen rather than to clarify the mystery of how these surface layer arrays have been acquired by so many bacteria and what the function of these layers might be in the natural habitat.

ACKNOWLEDGMENTS

LITERATURE CITED

1. **Amos, L. A., R. Henderson, and P. N. T. Unwin.** 1982. Three dimensional structure determination by electron microscopy of two-dimensional crystals. Prog. Biophys. Mol. Biol. **39:**183–231.
2. **Beveridge, T. J.** 1981. Ultrastructure, chemistry, and function of the bacterial wall. Int. Rev. Cytol. **72:**229–317.
3. **Buckmire, F. L. L., and R. G. E. Murray.** 1970. Studies on the cell wall of *Spirillum serpens*. I. Isolation and partial purification of the outermost cell wall layer. Can. J. Microbiol. **16:**1011–1022.
4. **Buckmire, F. L. L., and R. G. E. Murray.** 1976. Substructure and in vitro assembly of the outer, structured layer of *Spirillum serpens*. J. Bacteriol. **125:**290–299.
5. **Chang, J.-J., K. Leonard, T. Arad, T. Pitt, Y.-Y. Zhang, and L.-H. Zhang.** 1982. Structural studies of the outer envelope of *Chlamydia trachomatis* by electron microscopy. J. Mol. Biol. **161:**579–590.
6. **Deatherage, J. F., K. A. Taylor, and L. A. Amos.** 1983. Three-dimensional arrangement of the cell wall protein of *Sulfolobus acidocaldarius*. J. Mol. Biol. **167:**823–852.

7. Glaeser, R. M., W. Chiu, and D. Grano. 1979. Structure of the surface layer protein of the outer membrane of *Spirillum serpens*. J. Ultrastruct. Res. **66**:235–242.

8. Hayward, S. B., and R. M. Stroud. 1981. Projected structure of purple membrane determined to 3.7 Å resolution by low temperature electron microscopy. J. Mol. Biol. **151**:491–517.

9. Jaffe, J. S., and R. M. Glaeser. 1984. Preparation of frozen-hydrated specimens for high resolution electron microscopy. Ultramicroscopy **13**:373–378.

10. Karlsson, B., T. Vaara, K. Lounatmaa, and H. Gyllenberg. 1983. Three-dimensional structure of the regularly constructed surface layer from *Synechocystis* sp. J. Bacteriol. **156**:1338–1343.

11. Kellenberger, E., M. Häner, and M. Wurtz. 1982. The wrapping phenomenon in air-dried and negatively stained preparations. Ultramicroscopy **9**:139–150.

12. Murray, R. G. E. 1963. On the cell wall structure of *Spirillum serpens*. Can. J. Microbiol. **9**:381–392.

13. Shaw, P. J., and G. J. Hills. 1981. Tilted specimens in the electron microscope: a simple specimen holder and the calculation of tilt angles for crystalline specimens. Micron **12**:279–282.

14. Shaw, P. J., G. J. Hills, J. A. Henwood, J. E. Harris, and D. B. Archer. 1985. Three-dimensional architecture of the cell sheath and septa of *Methanospirillum hungatei*. J. Bacteriol. **161**:750–757.

15. Sleytr, U. B., and P. Messner. 1983. Crystalline surface layers on bacteria. Annu. Rev. Microbiol. **37**:311–339.

16. Taylor, K. A., J. F. Deatherage, and L. A. Amos. 1982. Structure of the S-layer of *Sulfolobus acidocaldarius*. Nature (London) **299**:840–842.